

SNR benefits of Surface Coil Lift-Off at High Magnetic Field Strength

Q. Duan¹, G. Wiggins¹, B. Zhang¹, R. Lattanzi¹, B. Stoeckel², and D. K. Sodickson¹

¹Radiology, Center for Biomedical Imaging, NYU School of Medicine, New York, NY, United States, ²Siemens Medical Solutions USA Inc., New York, NY, United States

Introduction

Optimal coil size and coil positioning are important concepts in MR coil design. For a single loop coil lying on a lossy infinite half-space [1, 2], the optimal coil size for a given depth in the sample has been thoroughly studied. In general practice, surface coils have been placed as close as possible to the body, emulating the arrangement most commonly studied in theoretical optimizations. However, Hayes and Axel [3] showed that for a comparatively large coil (14cm diameter) the SNR did not decrease appreciably as the coil was moved away from the tissue until the body noise no longer dominated. For high field strengths, furthermore, some coil designers have speculated about whether an offset of surface coils from the body might prove beneficial for SNR given the shifting balance of high-frequency electric and magnetic fields. Simulation work from Vesselle et al [4] suggested that for regions of interest near the center of a cylindrical phantom, an optimal lift-off position exists, and this optimal offset generally increases with increasing field strength. Though Vesselle et al validated these predictions with field measurements, their findings have not been confirmed to date in direct MR measurements. Furthermore, the Vesselle et al simulations did not include models of coil-derived noise, which is expected to represent an important determinant of SNR as coil offset increases. In this study, we identify regions and experimental conditions under which lift-off benefits exist for single loop coils, using two independent approaches: full wave simulations considering body-, coil-, shield-, and preamplifier-derived noise, and experimental SNR measurements on a 3T Siemens TIM system.

Methods

Phantom and Coils: A Siemens cylindrical water phantom with 16cm diameter and 36cm length was used. The phantom fluid has an electrical conductivity of $\sigma = 0.5$ S/m and a relative permittivity of $\epsilon_r = 79$. Seven lift-off positions from the phantom were tested: 1.3cm, 1.8cm, 3.0cm, 3.5cm, 4.0cm, 4.5cm, and 5.0cm. Two cylindrical window coils (i.e. flexible rectangular loops contoured to a cylindrical surface at each test radius) were built for the experiments: a 10cm x 10cm ("large") coil and a 6.2cm x 8.4cm ("small") coil.

Full Wave Simulations: Full wave electromagnetic simulations were performed for coil arrays and phantoms with cylindrical geometry using a dyadic Green's function formulation [2, 5]. Physical dimensions and dielectric properties were selected to match the phantom and the coils used in our experiments. In addition to body-derived noise, our noise model included noise derived from the coil conductor, the conductive shield (placed at a radius matching the RF shield radius in our TIM Trio system), and the preamplifiers (modeled using an experimentally determined noise figure) [5]. Determining the correct coil noise contribution required calibration of computed noise resistance against experimental measurements of loaded and unloaded resistance in the physically constructed coils. The need for this calibration reflects, in large part, the fact that at high frequency current is not uniformly distributed across the coil conductor but is concentrated at its edges – a phenomenon not automatically captured by our simulation method, in which the current distribution is specified as a starting point. Assumption of an approximate functional form for actual high-frequency current distributions yielded results generally consistent with our experimental calibrations. Simulated object resistance was also validated against bench tests in the actual phantom, yielding good agreement. As an additional validation of our simulation methodology, results presented by Vesselle et al [4] were reproduced identically when all noise sources except body noise were removed. Unlike in previous work [4] which explored several discrete points of interest within the object, full 2D SNR profiles with 1mm resolution were generated rapidly by evaluation of computed SNR along dense radial lines followed by interpolation. Both 2D SNR and SNR gain profiles were simulated at all lift-off positions for both coils.

MRI Experiments: A carefully designed coil holder was built to ensure accurate radial positioning while ensuring that the coil conformed to a cylindrical surface concentric with the cylindrical phantom. The coil was tuned and matched at each radial position. SNR measurements were performed using a GRE sequence (TR/TE/Flip = 2000/4.34/90, BW=180, 128x128, FoV 220mm), with careful calibration of body coil excitation. The noise level was measured with same sequence in the absence of RF excitation. Both 2D SNR and SNR gain profiles were then computed from the raw image data at all lift-off positions for both coils, using measured signal distributions and measured RF-free noise power in a manner directly matching the SNR computation algorithm used in the simulations.

Results

Contrary to the results of Vesselle, we did not observe any lift-off benefit at the center of the sample. However, at positions beyond the center of the phantom, such as the ROI indicated in Fig. 1, the existence of a concrete lift-off benefit was confirmed by experimental measurements. Fig. 1 shows SNR variation with position of the large coil for a point of interest deep in the object (indicated by the blue square). Fig. 2 demonstrates 2D SNR profiles and SNR gain profiles derived from simulations and determined experimentally for the same coil geometry. There is a very close match between simulation and experiment. Similar results were obtained for the small coil. The curling of the B_1^+ receive field at 3T is well depicted by the SNR profile. The specially designed colormap for the SNR ratios shows SNR gain in warm colors (e.g. red) and SNR loss in cold colors (e.g. green). From the 2D SNR gain profile, it is clear that, with all noise sources present, SNR at the near side of object dropped with coil lift-off whereas at points further from the coil SNR increased with coil lift-off until an optimal position was reached. The gain pattern is not symmetric due to the familiar twisting of B_1^+ and B_1^- at high field [6]. When all noise sources except body noise are excluded from the simulation (Fig. 3), lift-off benefit is observed over a larger area of the phantom, including in the center.

Discussions and Conclusions

This paper presents both computational and experimental validation of lift-off benefits for a single loop coil at 3T field strength. Curiously, the lift-off benefit is seen only on the far side of the phantom for this experimental setup. The absence of a lift-off benefit for the center of the phantom can be attributed primarily to the influence of coil noise, which was not included in Vesselle's original work, as well as to differences in coil and phantom dimensions. For the smaller coil, simulations considering only sample noise reproduce the central SNR boost with lift-off shown by Vesselle, though the area with greatest boost is still beyond the center of the phantom and displaced to one side (Fig. 3). The complex geometries and disparate electrical properties encountered *in vivo* are expected to perturb these findings somewhat, but for many body regions the general trends reported here may be expected to hold. The extremely close match between simulation and experiment in this work also suggests that our rapid simulation methods may be used with some confidence to guide future coil designs. The fact that SNR gains are observed primarily on the side of the object opposite to the coil element raises the question of what gains may be expected for encircling coil arrays, and studies related to this question are underway.

References

[1] Wang, et al, IEEE TBME 1995, 42:908-17. [2] Schnell, et al, IEEE TAP; 48:418-28. [3] Hayes et al, Med. Phys 1985, 12 :604-7. [4] Vesselle, et al, IEEE TBME, 42:507-20. [5] Lattanzi, et al, ISMRM 2008: 1074. [6] Collins, et al, MRM 2002, 47:1026-28

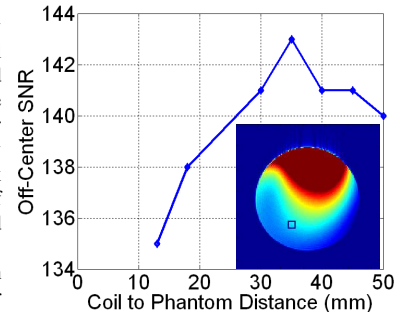


Fig. 1: Experimentally-measured SNR at a point deep within the object as a function of coil-to-phantom distance.

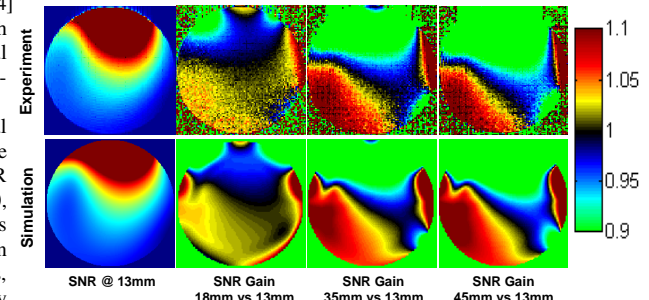


Fig. 2: Example 2D SNR profiles and SNR gain profiles for the large coil, determined by experiment (top row) and simulation (bottom row) at various radial locations.

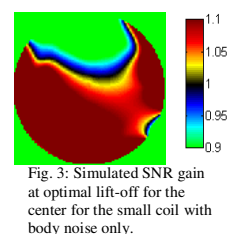


Fig. 3: Simulated SNR gain at optimal lift-off for the center for the small coil with body noise only.